minerals

MDPI

Article

Fit-for-Purpose Model of HP500 Cone Crusher in Size Reduction of Itabirite Iron Ore

Brena Karolyne Nunes da Rocha [1], Túlio Moreira Campos [1], Júlio Silva [2] and Luís Marcelo Tavares [1,*]

[1] Department of Metallurgical and Materials Engineering, Universidade Federal do Rio de Janeiro, Rio de Janeiro 21941-972, Brazil; brena.nrocha@metalmat.ufrj.br (B.K.N.d.R.); tulio.campos@coppe.ufrj.br (T.M.C.)
[2] Anglo American, Conceição do Mato Dentro 35860-000, Brazil; julio.silva@angloamerican.com
* Correspondence: tavares@metalmat.ufrj.br

Abstract: Cone crushers have a central role in the processing of quarry rocks, besides coarser ore preparation in several mineral processing plants. This is particularly true in the case of Itabirite iron ore preparation plants in Brazil, so optimizing their performance is of central importance for reaching maximum productivity of the circuit. The work presents results of modeling the HP500 cone crusher in operation in an industrial plant in Brazil (Minas Rio), from surveys carried out over a few years with different feeds and crushing conditions. A version of the Andersen–Whiten cone crusher model was implemented in the Integrated Extraction Simulator featuring a non-normalizable breakage response and a fit-for-purpose throughput model. The results demonstrate the good ability of the model to predict crusher performance when dealing with different closed-side settings and feed size distributions.

Keywords: cone crushing; modeling; simulation; iron ore

check for updates

Citation: Rocha, B.K.N.d.; Campos, T.M.; Silva, J.; Tavares, L.M. Fit-for-Purpose Model of HP500 Cone Crusher in Size Reduction of Itabirite Iron Ore. *Minerals* **2024**, *14*, 919. https://doi.org/10.3390/min14090919

Academic Editor: Pura Alfonso

Received: 10 August 2024
Revised: 30 August 2024
Accepted: 4 September 2024
Published: 7 September 2024

Copyright: © 2024 by the authors. Licensee MDPI, Basel, Switzerland. This article is an open access article distributed under the terms and conditions of the Creative Commons Attribution (CC BY) license (https://creativecommons.org/licenses/by/4.0/).

1. Introduction

Itabirite iron ores correspond to Banded Iron Formation (BIF) deposits, which are composed primarily of iron minerals such as hematite and magnetite, along with silicates and various carbonates that are widely found in the state of Minas Gerais (Brazil) [1,2]. These formations are generally classified as low-grade iron ores and exhibit varying degrees of weathering, depending on their depth relative to the topographic surface. This depth-dependent weathering results in different typologies of Itabirite, each characterized by distinct mineralogical and textural features [1]. In general, Itabirite iron ores present characteristics that affect their size reduction response, with segregation in selected size classes [1,3–5], often associated with some extent of preferential mineral liberation by grain-boundary breakage [1]. This fracture behavior poses an additional challenge for describing the size reduction of these iron ores within crushing stages in a circuit simulation.

Itabirites located in the Iron Quadrangle (*Quadrilátero Ferrífero*) province are often reduced in size through a combination of multiple stages of crushing followed by ball milling [6]. Given the important role of crushing, proper selection and assessment of crushing circuits demands a deep understanding of the ore breakage behavior since it impacts the overall productivity and cost-effectiveness of mining projects. Despite the large experience in the minerals industry in designing crushing circuits, challenges in this comminution stage are still a reality for processing Itabirite iron ores [1].

Important advances have been made in the understanding and modeling of size reduction in cone crushers in the last 50 years or so. Whiten [7] proposed a model to describe compressive crushing from the classification and breakage functions, which became the most well known in the field [8]. This modeling approach relies on fitting these functions based on data, typically obtained from industrial surveys of crushing circuits, where the key parameters of the classification function are often linearly related to the crusher closed-side

setting (CSS). Such applications of the model were previously demonstrated in modeling the performance of standard Symons and short-head cone crushers in the size reduction of limestone [9] and uranium ore [10]. More recently, Neves and Tavares [11] modeled Hydrocone crushers in the size reduction of gneiss.

Andersen and Napier-Munn [12] then proposed modifications to Whiten's model by incorporating a breakage (appearance) function that is obtained from single-particle breakage tests and a method to predict crusher power. This has the advantage of reducing the number of parameters that require fitting, besides establishing a connection between the single-particle breakage response and crusher power during operation. They used this model to describe size reduction in a Symons short-head cone crusher [12], and linear variations of the key parameters in the classification function were established not only for the CSS, but also for eccentric throw, throughput, 80% passing in the feed and liner condition. Moshgbar et al. [13] used this model incorporating the rate of wear of the concave and mantle liners to transform the classification function parameters into time-dependent functions. Magalhães and Tavares [14] then used the model to back-calculate breakage characteristics of ore samples from tests in a laboratory cone crusher. More recently, an adapted version of the model was used to describe industrial cone crushing with different values of the CSS [15].

Alternative models of cone crushers have been proposed using other population balance model approaches [16,17], besides a mechanistic model [18] and, more recently, the Discrete Element Method (DEM) [19–22]. The mechanistic model of Evertsson [18], which describes the effect of CSS, chamber geometry, eccentric throw and eccentric frequency, has been proposed as a model suitable for design but lacks fitting parameters to represent a particular operation. On the other hand, the DEM is a powerful tool for analyzing these and other variables in crushing but is not suitable for circuit simulation.

Another important aspect of cone crusher simulation is the prediction of throughput when operating with a filled chamber (choke-feeding). Gauldie [23] proposed a theoretical throughput model for cone crushers, which accounts for crusher geometry, speed and liner configuration, which was later improved [24]. Karra [9] proposed an empirical model that described the variation in crusher capacity as a function of eccentric throw, CSS and head angle.

The present work initially proposes minor modifications to Whiten's crusher model to account for non-normalizable breakage behavior that is found in cone crushing of Itabirite iron ores, besides expressions to identify maximum crusher capacity. Fitting of model parameters from data collected over several years of operation of HP500 cone crushers in the Minas Rio crushing plant in a secondary crushing role is then carried out.

2. Modelling Background

2.1. Andersen–Whiten Crusher Model

Whiten's model [7] describes the compressive crushing of ore particles as a size–mass balance in different size classes by successive stages of classification and particle breakage. The overall product size distribution in distributed form (p) can be predicted as follows [25]:

$$p = (I - C)(I - BC)^{-1} f \tag{1}$$

where I is the identity matrix, f is the feed size distribution vector, B is the lower-triangular breakage function matrix, and C is the classification function, represented by a diagonal matrix.

The classification function defines the probability of a particle in a given size range being classified for breakage and is given as follows [25]:

$$\begin{array}{cc} C(\overline{x}) = 0 & \overline{x} \le K_1 \\ C(\overline{x}) = 1 - \left(\frac{K_2 - \overline{x}}{K_2 - K_1}\right)^{K_3} & K_1 < \overline{x} < K_2 \\ C(\overline{x}) = 1 & \overline{x} \ge K_2 \end{array} \tag{2}$$

where model parameter $\overline{x}$ is the representative size given by $\overline{x} = \sqrt{x_i x_{i-1}}$, where x_i represents the sieve size i. Parameter K_1 defines the bottom limit of the middle portion of the distribution curve described by Equation (2), which defines the particle size below which particles are not nipped by the crusher. Parameter K_2 defines the upper limit of the distribution curve, which determines the size above which all particles are nipped. Parameter K_3 defines the slope of the curve. The optimal values of K_1 and K_2 depend on the operating conditions of the crusher, feed characteristics and machine settings. Empirical relationships have been proposed between them and the cone crusher variables, giving [25]

$$K_1 = A_0 + A_1 CSS + A_2 Q + A_3 f_{80} + A_4 LLEN \quad (3)$$

$$K_2 = B_0 + B_1 CSS + B_2 Q + B_3 f_{80} + B_4 LHR + B_5 ET \quad (4)$$

where CSS is the closed-side setting, Q the crusher throughput, f_{80} the 80% passing size in the feed, $LLEN$ the thickness of the mantle liner, LHR the mantle operating time, ET the eccentric throw and A_0 to A_4 and B_0 to B_5 are model fitting parameters. K_3 is often assumed as a constant value of 2.3 [25], although Karra [9] found that the optimal value was 3.0.

Particles that are classified for breakage in Equation (2) will be compressed down to the CSS and eventually break. Whiten's model was later modified to use the appearance function obtained from single-particle breakage tests [12], using the t_{10}-t_n relationship [26]. The appearance function method is well known for its use in energy-based modeling, but it is assumed to be a function of the crushing operating conditions as [25]

$$\mathrm{t_{10}} = \mathrm{D_0} - \mathrm{D_1 CSS} + \mathrm{D_2 Q} + \mathrm{D_3 f_{80}} \quad (5)$$

$$B_{ij}{}' = \mathrm{interp}\left[t_{10}, t_n, x_i/x_j\right] \quad (6)$$

where D_0 to D_3 are fitting parameters and t_{10} and t_n are, respectively, the percent passing in $1/10$th and $1/n$th of the parent particle size. The effect of size on breakage resistance can be taken into account by using drop-weight data for particles contained in different size ranges.

To calculate the crusher power (P_c) during operation, Andersen and Napier-Munn [12] proposed a model that is based on the no-load power of the crusher and the power estimated from the impact test, originally conducted using the pendulum test and more recently using the drop-weight test, as follows:

$$P_c = \zeta P_d + P_n \quad (7)$$

where P_n is the no-load power (kW), ζ is a dimensionless factor for a specific crusher and P_d is the power estimated based on drop-weight tests given as follows [25]:

$$P_d = Q \sum_{i=1}^{N} Ecs_{t10_i} C_i w_i \quad (8)$$

where w_i is the mass fraction of material in each size in the crusher, N is the number of size classes and Ecs_{t10_i} is the energy matrix compiling the specific energy required to generate a t_{10} equal to 10%, 20% or 30%, which allows describing the effect of particle size on impact strength [25]. The DWT power from Equation (8) assumes that the work performed by the crusher is a function of the energy required to break the particles from the feed that were classified for breakage, with a given efficiency ($1/\zeta$), besides the no-load power.

2.2. Adaptations to the Crusher Model

With the aim of further improving the applicability of the Andersen–Whiten model [7,12] for the Itabirite iron ore in question, some modifications were implemented in the present work. At first, a modification was introduced to account for the non-normalizable character

of the breakage (appearance) function with respect to size. A second modification consisted in the estimation of the maximum throughput of the crusher when operating with a full chamber as a function of feed and operating conditions.

As extensively reported for processing Brazilian Itabirite iron ores [1,3–5] and already discussed, the breakage behavior of the ore may follow a size distribution that is non-normalizable with respect to the original particle size. A simple and effective way to account for this feature was proposed elsewhere [27] and was recently used by population balance modeling [3–5,28,29] and mechanistic breakage modeling [30]. The approach is given as follows [27]:

$$B_{ij} = {B_{ij}}' \left(\frac{x_i}{y_0} \right)^{n_3} \quad \text{for } x_i < y_0 \tag{9}$$

where ${B_{ij}}'$ is the cumulative breakage function given by Equation (6). By considering n_3 and y_0 equal zero, the breakage function in Equation (9) will rely on the breakage function predicted from Equation (6).

Cone crushers can operate at different feed throughputs, and these values directly affect crusher performance, as suggested in Equations (3)–(5). However, a maximum throughput is reached when the crusher operates with a filled chamber. Knowledge of this value is important when simulating the cone crusher in either dynamic or steady-state conditions since a mismatch between it and the feed throughput would define either the need to interrupt, at times, crusher feed to allow a minimum hopper level to be reached for choke-feeding operation or to divert part of the crusher feed to a crusher next to it, when that is the case. Empirical evidence has been compiled from data collected by cone crusher manufacturers over a century of operation of these machines regarding the effect of variables on this maximum throughput. Such evidence has been compiled in the past in crushing manuals [31], but it is now built into simulators such as Bruno© from Metso [32] and PlantDesigner© from Sandvik. They show that maximum cone crusher throughput (Q_{max}) is a function of closed-side setting (CSS), feed size (f_{80}), bulk ore density (ρ_a), ore competence (impact work index—Wi) and feed moisture (ω).

A reverse engineering approach was adopted to define relationships between some of the variables listed above and the maximum throughput of the crusher. Simulations were run with Bruno© (Version 4.2.2.0, exe v4.1.2.9, DB v9.50, Metso Corporation), while crusher manufacturer´s tables were analyzed [31] by investigating the effect of one variable at a time. A base case was defined following the default material as suggested in Bruno©, which is a granite with specific gravity (ρ_{sp}) of 2700 kg/m^3, with bulk density (ρ_a) of 1600 kg/m^3 and a Wi value of 16 kWh/t. The feed was considered with a moisture content of 1% and the 80% passing size of 100 mm, while the HP500 crusher was set to a nominal CSS of 38 mm with a medium cavity. The maximum crusher throughput can be defined through an empirical relationship, which is modified from a preliminary version presented in the crusher manuals [31]:

$$Q_{max} = \lambda Q_T \alpha \beta \gamma \delta \Psi \tag{10}$$

where α, β, γ, δ and Ψ are correction factors, equal to 1 for the base case, varying as a function of ore bulk density, resistance to crushing, feed size, moisture content and closed-side setting, respectively. Q_T is the crusher capacity of the base case, and λ is a dimensionless fitting parameter that should be fitted to the industrial data available.

The correction factor for the effect of ore bulk density (α) is simply given by

$$\alpha = \frac{\rho_a}{1600} \tag{11}$$

where ρ_a is the ore bulk density, given in kg/m^3. The correction factor for resistance to crushing is calculated by

$$\beta = \left(\frac{16}{Wi} \right)^{\eta} \tag{12}$$

where Wi is the impact work index [33,34], given in kWh/t, and η is a fitting parameter. The contribution of the feed coarseness is given as

$$\gamma = \left(\frac{100}{f_{80}}\right)^{\ni} \tag{13}$$

where f_{80} is the 80% passing size in the feed, given in mm, and $\ni$ is a fitting parameter. The correction factor that accounts for the moisture content is

$$\begin{array}{cc} \delta = 1 & \text{for } \omega < 1\% \\ \delta = \exp[-\xi(\omega - 1)] & \text{for } \omega \geq 1\% \end{array} \tag{14}$$

where ω is the feed moisture content (%) and ξ is a fitting parameter. Care should be taken when using Equation (14) since the relevant moisture is the one contained in the crusher feed, which is often lower than that of the ROM ore.

Finally, the contribution of the closed-side setting is given as

$$\Psi = \left(\frac{CSS}{CSS_{BC}}\right)^{\nu} \tag{15}$$

where CSS and CSS_{BC} are, respectively, the closed-side setting for the crusher in operation and the closed-side setting of the base case, given in mm, while ν is a fitting parameter.

In the case of the HP500 crusher, the capacity of the base case (Q_T) becomes equal to 647 t/h according to Bruno© [32]. The final parameter to be calibrated is λ, which is estimated on the basis of at least one relevant measurement of throughput when the crusher is operating under choke-fed conditions. Other effects, such as chamber type, eccentric throw, clay content and wear condition of the liner, are also known to affect the maximum throughput of the cone crusher [21,24,33]. The model corresponding to Equations (10)–(15) assumes that these need to be accounted for in the fitting parameter λ since they are not explicitly represented in the equations.

3. Methodology

3.1. Experimental Section

The work was focused on the secondary crushing stage of the Minas Rio Plant, operated by Anglo American and located in Conceição do Mato Dentro (Minas Gerais, Brazil). The Run-of-Mine ore is composed of four different iron ore lithologies, named Friable, Compact and Supercompact Itabirites, and Canga. Such lithologies were previously characterized according to their liberation and breakage response, being composed mostly of hematite and quartz [1]. While the feed is represented by a blend of these ores, the significantly finer feed size of Friable Itabirite, besides the small amount of Canga in the Run-of-Mine (<5%), allows us to consider that the cone crusher is fed by a blend of Compact and Supercompact Itabirites. The mean specific gravity of these, measured by pycnometry, was estimated as 3480 kg/m^3. The bulk (apparent) density was measured by placing each weighed sample in a beaker and measuring the bulk volume after vibration, being given as 2088 kg/m^3.

The secondary crushing stage, represented by four HP500 crushers, is fed by two primary jaw crushers. The cone crushers operate in a closed circuit with vibrating screens with 25 mm openings, whose undersize is fed to HPGRs.

The crushers are installed in parallel, making it possible to alternate their use according to different operational demands. All crushers were designed with a nominal closed-side setting (CSS) of 38 mm, installed power of 355 kW and maximum feed particle size of 204 mm, owing to the medium cavity of the crusher used [32]. A total of ten industrial surveys were carried out over three years of operation, and a summary of operating conditions and feed characteristics of each survey is presented in Appendix A (Table A1). The range of operating conditions varied from a CSS of 38 to 54 mm and from an 80%

passing size in the feed (f_{80}) of 47 to 140 mm. All surveys were considered to be conducted with the crushers operating with a full chamber.

Representative samples of the feed and product of the cone crusher were collected from belt cuts in the surveys after the crash-stopping of the operation. Operating conditions, including CSS, solid feed rate and crusher power were recorded from the supervisory system for each survey. All samples were split, and their particle size distribution was analyzed by dry sieving in a RoTap® sieve shaker.

The ore breakage characterization of representative samples of Compact and Supercompact Itabirites was conducted through drop-weight tests (DWTs) [25] and the Bond impact crushability (Wi) test [33,34]. In the first, narrow size samples contained in size ranges of 13.2–16.0 mm to 53.0–63.0 mm were impacted at stressing energies varying from 0.05 to 2.5 kWh/t, and their size distribution was analyzed by sieving. Markers from the size distributions, representing the proportions passing 1/2, 1/4, 1/10, 1/25, 1/50 and 1/75th of the initial particle sizes, called t_n markers [26], were calculated. Relationships between the stressing energy and the percent passing 1/10th of the initial size (t_{10}), and between this parameter and the various t_n values were then recorded. Additionally, the Bond impact work index was estimated based on the standard test from a selection of 70 particles contained in the size range of 53.0–75.0 mm for each ore type [34].

3.2. Model Implementation and Calibration

The crusher model presented in detail in Section 2 was implemented in the commercial software Integrated Extraction Simulator (IES) (Orica Inc., Victoria, Australia) to perform steady-state simulations.

The appearance or breakage function was described using the t_{10}-t_n relationship. Data were interpolated using the incomplete beta function [35], with the non-normalizable breakage correction term (Equation (9)) used to describe the breakage (appearance) function. On the other hand, parameters of the classification function (Equation (2)) were, at first, fitted based on results from each industrial survey. Thus, based on the appearance function (t_{10}-t_n) from the DWT tests, the present work calibrated the classification function parameters (Equations (2)–(4)) and the t_{10} (Equation (5)) to data from each industrial survey. Parameters of these equations were fitted separately to data from each industrial survey using the IES platform.

The ultimate goal of the work was to obtain a single set of parameters to describe all industrial surveys, which would enable the simulation of the plant under different operating conditions and feed characteristics. As there was a significant difference in the CSS and 80% passing sizes of the feed in the industrial surveys, the present work fitted Equations (2)–(5) considering these two operating variables. Information on the wear condition of the liners was not available, so it could not be included in the model, besides minor variations in ore composition. The optimal parameters fitted for each industrial survey were then used as part of the multiple regression to obtain the final set of parameters that would allow representing a compromise between simplicity in modeling and fidelity in representing the survey data. Finally, all parameters were used to simulate the industrial campaigns.

4. Results

4.1. Breakage Characterization

As mentioned in Section 3.1, the two ore types that predominate in the feed to the secondary crushing stage, namely the Compact and the Supercompact Itabirites, have been subjected to testing separately in order to assess their breakage response. The amenability of the iron ore lithologies to impact breakage was analyzed by inspecting the relationship between the t_{10} and the specific impact energy. The results are summarized in Figure 1 and clearly present a steep reduction in breakage intensity for specific energies below 1 kWh/t, while breakage saturation is reached above this point. The results also show the higher values of t_{10} for comparative impact energies for the Compact Itabirite when compared

to the Supercompact Itabirite, which highlights the lower amenability for breakage of the latter.

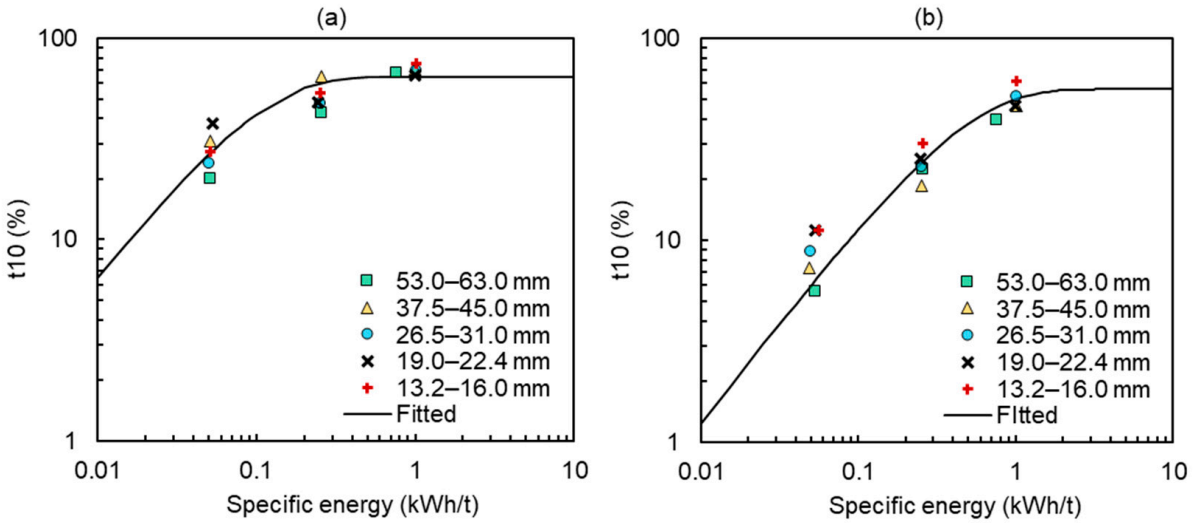


Figure 1. Relationship between t_{10} and the specific impact energy for different narrow size ranges of Compact (**a**) and Supercompact Itabirites (**b**) tested in the DWT.

The results from Figure 1 may be described mathematically as follows [26]:

$$t_{10} = A\left[1 - \exp\left(-bE_{sp}\right)\right] \quad (16)$$

where E_{sp} is the specific energy and A and b are fitting parameters. The optimal values of parameters from Equation (16) used to describe the data presented in Figure 1 are listed in Table 1. The product of the values ($A \times b$), which represents the derivative of Equation (16) with respect to the specific impact energy (E_{sp}) when its value is equal to zero, is often used to characterize the amenability for breakage of different materials [25]. The values found for the ore types demonstrate their higher amenability to breakage when compared to other materials [36].

Table 1. DWT breakage model parameters and impact work index of the ore types.

Ore Type	*A*	*b*	$A \times b$	*Wi* (kWh/t)
Compact Itabirite	64.5	10.5	677.3	7.2
Supercompact Itabirite	56.1	2.20	123.4	10.6

A more detailed examination of results from drop-weight tests for selected size ranges is presented in Figure 2, which shows the product size distributions from DWTs for the narrow size ranges of 37.5–45.0 mm (a) and 26.5–31.0 mm (b) for Compact Itabirite under different specific energies. The graphs highlight the significant non-normalizable breakage behavior of this Itabirite iron ore, which is identified by the inflection point, highlighted by the red arrow, at around 240 µm for the different narrow size ranges tested.

In addition, the relationship between the values of t_{10} and the various values of t_n [26] has also been obtained. The results from all narrow size ranges tested are presented in Figure 3 for the two ore types, showing that they were reasonably well grouped for mapping the breakage behavior of the material investigated in the present work, irrespective of the ore blend fed to the crusher. The construction of this graph only included data for particle sizes above 240 µm, which was identified as the lower limit for the validity of the normalizable response (Figure 2).

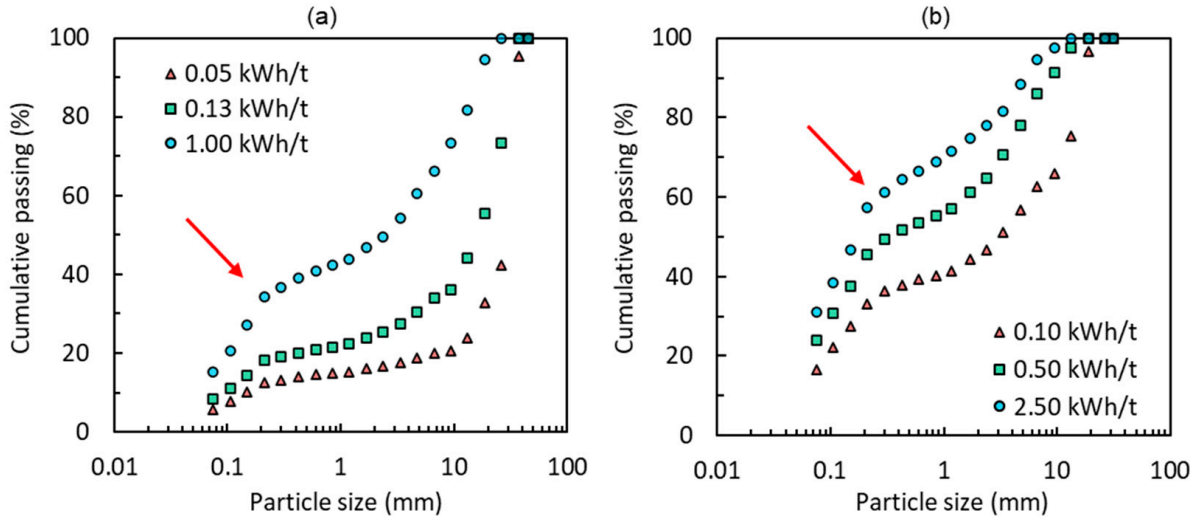


Figure 2. Product size distributions for DWTs under different specific energies in the narrow size range of 37.5–45.0 mm (**a**) and 26.5–31.0 mm (**b**) for the Compact Itabirite. The red arrow highlights the inflection around 240 μm.

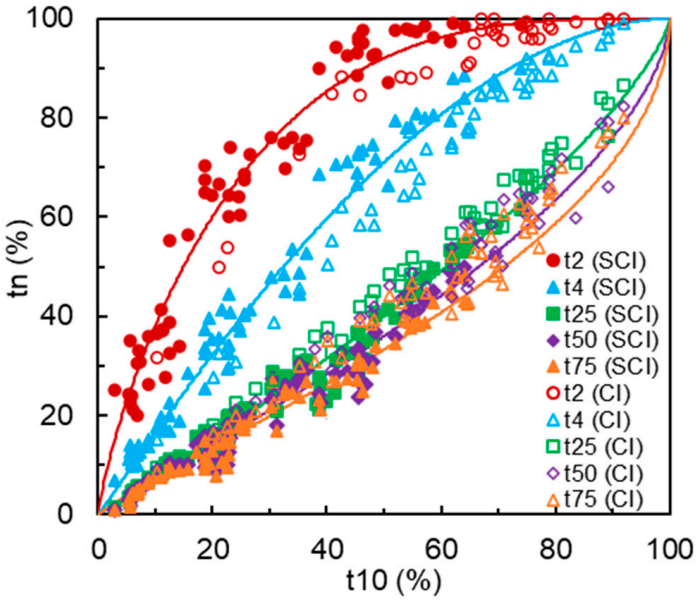


Figure 3. Appearance function (t_{10}-t_n relationship) from the DWTs for the iron ore samples investigated in the present work: Supercompact Itabirite (SCI) (filled symbols), Compact Itabirite (CI) (void symbols). Lines represent the fit to the incomplete beta function.

The results from Figure 3 are well described by the incomplete beta function [34], given by

$$t_n(t_{10}) = \frac{100}{\int_0^1 x^{\alpha_n-1}(1-x)^{\beta_n-1}dx}\int_0^{t_{10}} x^{\alpha_n-1}(1-x)^{\beta_n-1}dx \quad (17)$$

where α_n and β_n are fitting parameters. The optimal parameters from Equation (17) are listed in Table 2, while Figure 3 demonstrates the reasonable agreement between experimental and fitted values for each t_n analyzed.

Table 2. Summary of the incomplete beta function parameters fitted for each t_n for the Itabirite iron ore samples for particle sizes above 240 μm.

t_n	α_n	β_n
t_2	0.73	3.20
t_4	1.03	1.83
t_{25}	0.99	0.73
t_{50}	0.94	0.60
t_{75}	0.88	0.52

The Whiten crusher model uses tabulated values relating selected t_{10} values to the various t_n values, and the data are listed in Table 3. Standard values from Table 3 were obtained by interpolation using the incomplete beta function (Equation (17)) with optimal parameters from Table 2. Values from Table 3 are used internally by the model to estimate the breakage function from Equation (6), which is performed by spline interpolation.

Table 3. Summary of the appearance function (t_{10}-t_n relationship) for selected values of t_{10} used as an input for the Whiten crusher model.

t_n	t_{75} (%)	t_{50} (%)	t_{25} (%)	t_4 (%)	t_2 (%)
10	7.69	7.93	7.98	16.16	27.96
20	14.44	15.54	15.90	31.82	51.63
30	21.13	23.24	23.97	46.27	69.54

The Bond impact work index results, measured using Bond's procedure [33,34], are plotted in Figure 4, while average values are listed in Table 1. The distributions in the figure presented a high coefficient of variation (around 50%), with values varying from 1.9 to 15.5 kWh/t and 3.6 to 26.7 kWh/t for the Compact and Supercompact Itabirites, respectively.

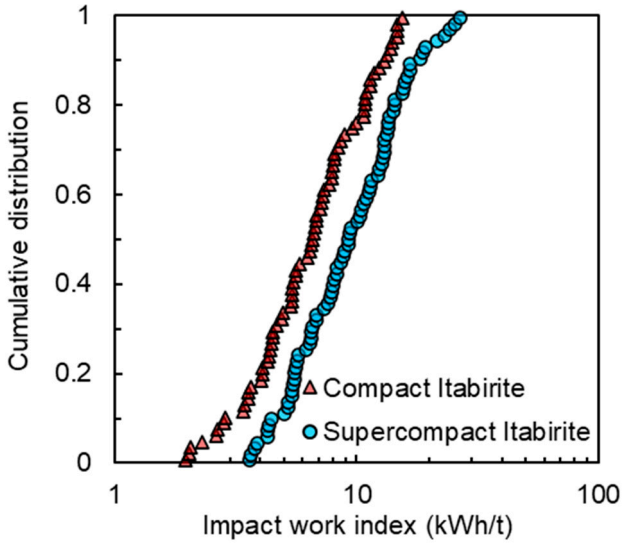


Figure 4. Distributed data from impact work index measurements for Compact and Supercompact Itabirite samples.

4.2. Industrial Surveys

Figure 5 presents the feed size distributions of all surveys performed with the cone crusher. The significant variation in feed top size is evident. In addition, large proportions of fines were observed in the feed in selected surveys, suggesting poor screening efficiency in the respective operations depicted in the surveys. Experimental campaigns with operations

close to ideal classification exhibited steep size distributions with particles mostly contained in the size range between 100 and 25 mm.

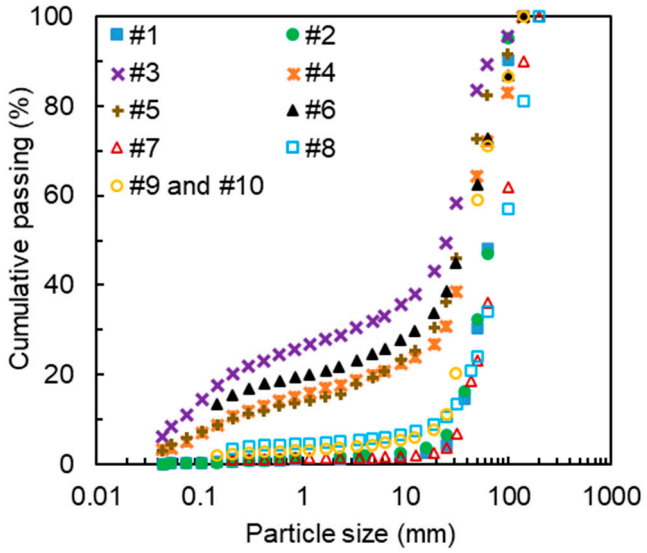


Figure 5. Feed size distributions of the cone crushers in all industrial surveys.

Figure 6 summarizes the measured product size distributions from samples of the various surveys. They show clear non-normalizable breakage behavior with segregation of particles in the range between approximately 500 and 100 µm, whereas data from breakage tests identified the inflection at 240 µm (Figure 2). Minor differences could be observed in the slope of the non-normalizable region in Figure 6. This same non-normalizable breakage behavior has been observed elsewhere for some other iron ores [37], quarry rocks [38] and platinum ores [39], and its mathematical description does not follow the original normalized breakage function [40] or normalized appearance function [26].

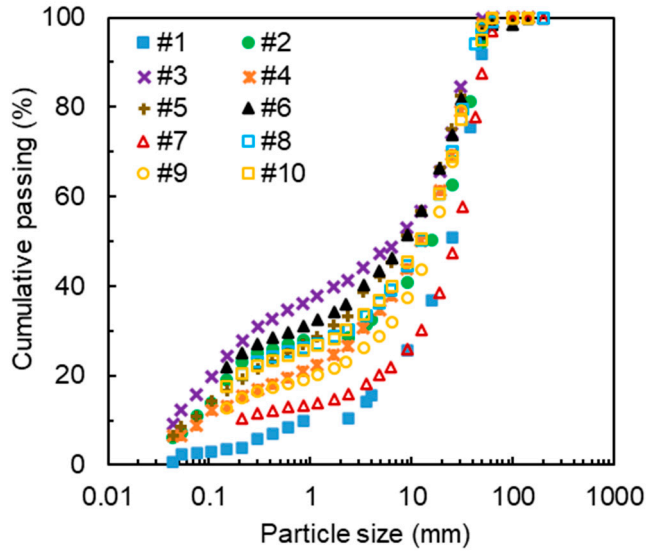


Figure 6. Product size distributions of the cone crusher for all industrial surveys.

A comparison of the values of 80% passing sizes in the feed and the product from the individual surveys demonstrates that the reduction ratio varied from 1.6 to 4.4, which is within the lower range of typical operation of cone crushers [41]. Such variations evidence the significant effect of the CSS and the feed size distribution in the different surveys (Table A1).

4.3. Model Fitting

Values of parameters in the sub-models describing the effects of impact work index, feed size, moisture and CSS on crusher throughput have been fitted to data, and a comparison is presented in Appendix B. A comparison between measured the fitted values in Figure 7 shows that Equation (10) was able to fit the data appropriately, with a mean sum of squares of the absolute relative deviations of 0.23, besides highlighting that both model predictions and experiments are within the limits defined by Bruno© for the coarser (green line) and finer (blue line) feed size distributions. Such deviations may be explained by variations in liner condition and feed blends. A summary of model parameters is presented in Table 4, where the optimal value of parameter λ was obtained based on industrial survey #10 (Table A1).

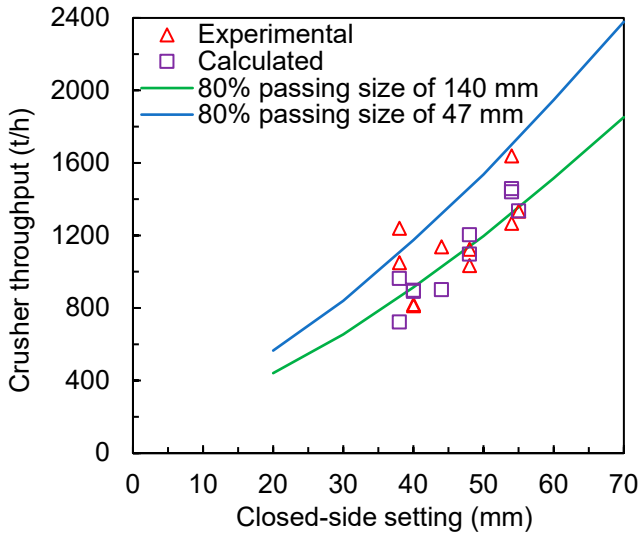


Figure 7. Comparison between experimental and calculated maximum crusher throughputs for all industrial surveys. Lines represent the limits of the crusher capacity for the coarser and finer feeds in the surveys.

Table 4. Values of parameters of the throughput model (Equation (10)) for the HP500 crusher in size reduction of Itabirite iron ore.

Sub-Model	Parameter	Value
Work index	η	0.15
Feed coarseness	$\ni$	0.26
Feed moisture	ξ	0.09
Closed-side setting	υ	1.27
Throughput model	λ	0.84

Based on the appearance function in Table 3, the present work then fitted the classification function parameters (Equation (2)) and the value of t_{10} for each industrial survey performed in the present work (Table A1). The model was fitted to describe the parameters K_1, K_2 and t_{10}, whereas parameter K_3 was kept constant at 2.3 as suggested elsewhere [24].

A comparison between the model and the experiments is first presented in Figure 8 for industrial survey #8 (Table A1), comparing the model fit considering the standard normalizable and the non-normalizable breakage function for particles below 240 μm (Mod. Whiten's model in the figure). It shows the importance of incorporating the modified breakage function for the particular iron ore in order to reach a good fit to data at fine sizes. The optimal values of parameters defining the non-normalizable breakage function (Equation (9)) were n_3 = 0.47 and y_0 = 0.24 mm.

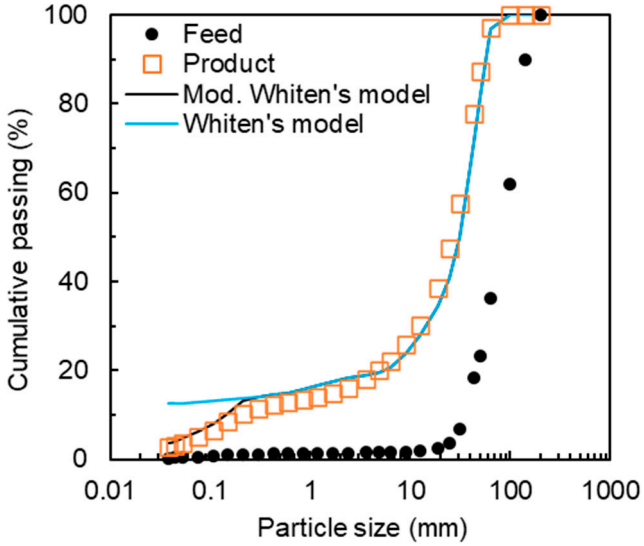


Figure 8. Comparison between experimental and simulated product size distributions using Whiten's crusher model and the modified model (Mod. Whiten's model in the figure) with the non-normalizable breakage function for industrial survey #8.

A comparison of data from selected surveys (#9 and #10) is presented in Figure 9, showing the good fit of the model to data for the crusher operating with the same feed, but different CSS values. The good agreement between the model and experiments highlights the robustness of the model and its ability to extrapolate its predictions to different operating conditions.

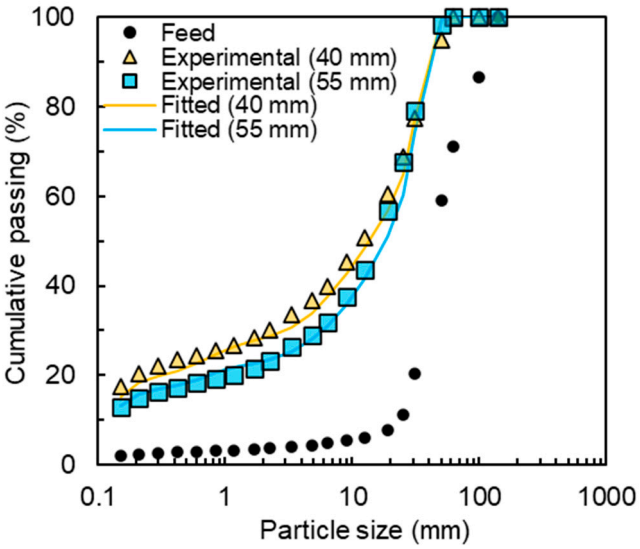


Figure 9. Comparison of model predictions and experiments for industrial surveys #9 and #10 with a single feed size but different CSS values.

A general comparison between experimental and fitted values for the percent passing 12.5 mm is presented in Figure 10 for all industrial surveys performed in the present work and highlights the good agreement between the model and experiments in the coarse part of the product size distribution. However, it is worth noting that different sets of parameters were used in fitting data from most industrial surveys.

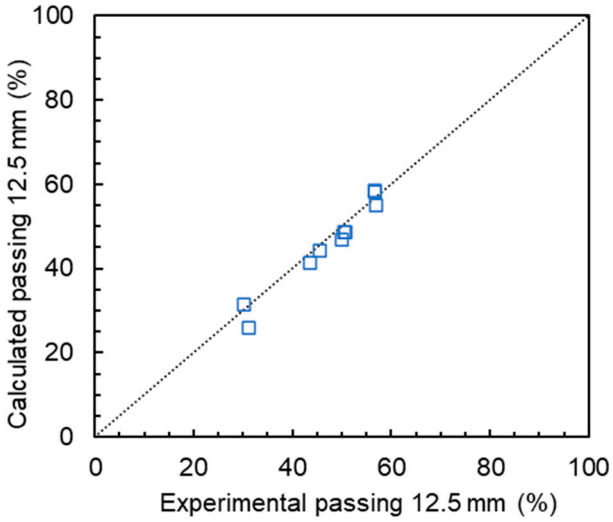


Figure 10. Comparison between experimental and fitted values for the percent passing 12.5 mm in the crusher product for the industrial surveys.

To obtain a set of parameters that describes the breakage behavior across all surveys, multiple linear regression was performed for each value of K_1, K_2 and t_{10} as a function of CSS and f_{80} to fit parameters in Equations (3)–(5). Satisfactory correlations were obtained for the t_{10}, K_1 and K_2 parameters, and optimal values are presented in Table 5. The results show that K_1 and K_2 increase with CSS, which is indeed the parameter that predominantly characterizes this effect in the classification for breakage.

Table 5. Optimal parameters for the Andersen–Whiten crusher model to describe results from industrial surveys performed in the present work.

Function	Parameter *	Value
Classification function K_1	A_1	0.23
	A_3	0.30
Classification function K_2	B_0	12.0
	B_1	0.55
	B_3	0.40
Appearance function t_{10}	D_0	64.0
	D_1	0.12
	D_3	−0.23
Power	P_n	110 kW
	ζ	1.30

* Absent parameters are equal to zero.

Since all tests were run under choke-feeding conditions, no dependence on throughput appeared ($A_2 = B_2 = 0$). Parameters K_1 and K_2 also increased with 80% passing size in the feed. The t_{10} value decreased with CSS and 80% passing size in the feed. The optimal value for the parameter A_1 (Equation (3)) is similar to the optimal values of 0.80 found by Karra [9], 0.65 by King [10] and 0.60 by Neves and Tavares [11]. This comparison shows that the final set of parameters proposed in the present work is in general agreement with previous applications of the model, in which K_1 (Equation (2)) is often 20% to 70% lower than the CSS. For parameter B_1 (Equation (4)), the optimal value was slightly lower than the usual range observed in some of the previous studies: 1.72 for Karra [9], 1.70 for King [10] and 1.45 for Neves and Tavares [11]. These differences in magnitude are explained by the strong dependence of parameter K_2 (Equation (2)) with respect to the 80% passing size in the feed, which was taken into account in the present work and not in the cited studies [9–11].

To demonstrate the validity of the set of values proposed in Table 5 describing the parameters fitted separately for each industrial survey campaign (Table A1), a comparison is presented in Figure 11. The results show good agreement between fitted and predicted values for the classification function parameters (K_1 and K_2 in Figure 11a) and for the breakage function parameter (t_{10} in Figure 11b). The results in Figure 11a also show the clear difference in magnitude between parameters K_1 and K_2. The values of parameter t_{10} in Figure 11b varied from 20% to 50%, which is higher than the usual range observed for secondary crushing stages [25]. Nevertheless, the results presented in Figures 1 and 3 highlight the high values observed for the t_{10} when processing Compact Itabirite, which partially explains the large values observed in Figure 11b.

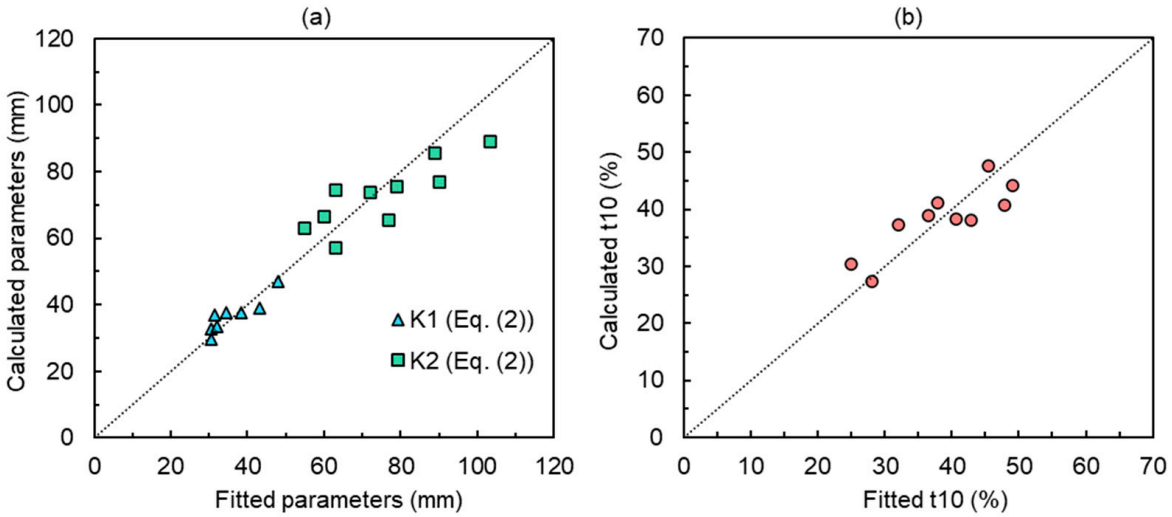


Figure 11. Comparison between predicted (calculated) and fitted values for the classification function parameters (**a**) and the t_{10} parameter (**b**). Predicted values were calculated from Equations (3)–(5) with the set of parameters in Table 5 and operating conditions for each industrial survey campaign (Table A1).

A comparison between the experimental and predicted product size distributions for selected industrial surveys is presented in Figure 12. The red line in Figure 12 shows the fitted values for each industrial survey, highlighting the good agreement between the model and experiments, as already shown in Figure 10. Simulated values using the set of parameters presented in Table 5 show good agreement between the model and experiments, with the model prediction slightly overestimating the coarse part of the product size distribution for industrial survey #3 (Figure 12b) and slightly overestimating data from industrial survey #8 in the fine part of the product size distribution (Figure 12d).

The validity of fitting parameters in Table 5 is again demonstrated in Figure 13 for a comparison of experimental and predicted percent passing 12.5 mm, as previously shown in Figure 10 for fitting each industrial survey separately. The agreement between the experimental and simulated results was reasonably good, although not as good as that in Figure 10. This is not surprising, given that the variations in liner conditions, moisture contents and crushability could not be accounted for explicitly in the modeling approach. The absolute relative deviation from measurements was up to 15%.

Finally, the parameters of the power model are also listed in Table 5, and a comparison between measurements and simulations is presented in Appendix C, which showed only fair agreement, likely associated with issues during the measurement of power from the different crushers operating in parallel.

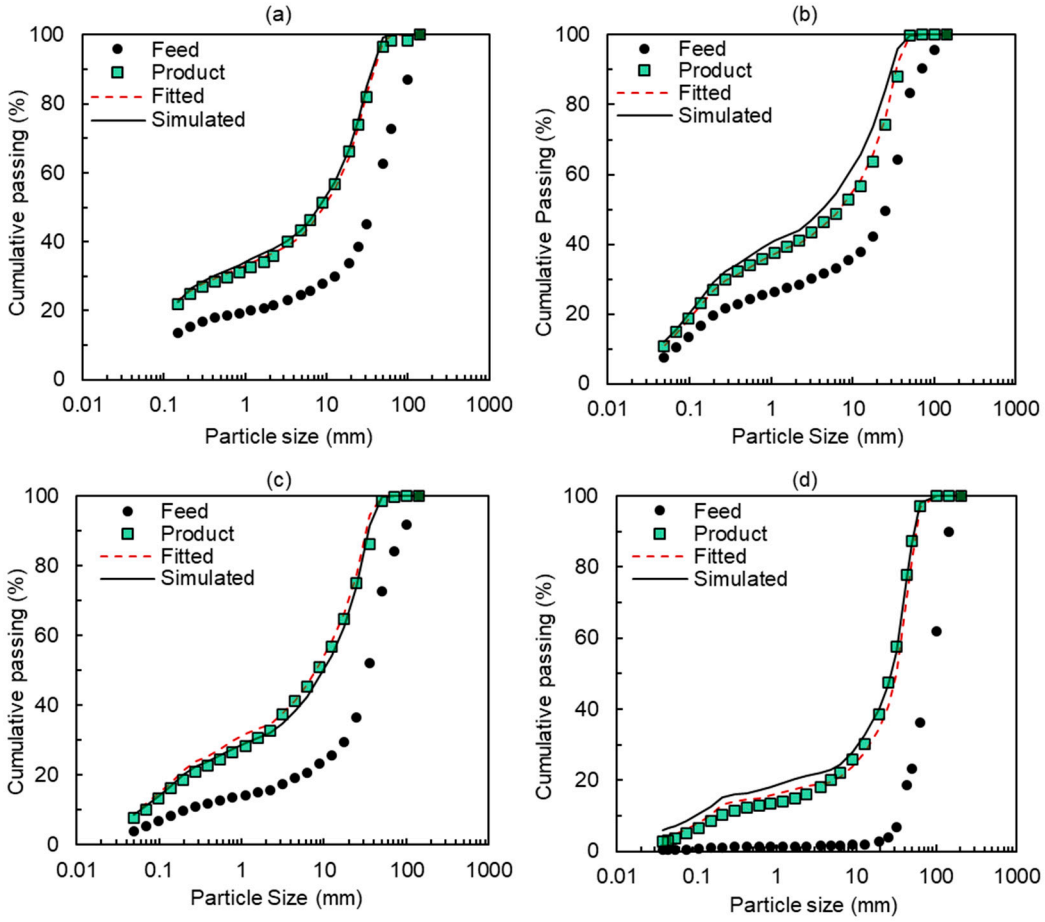


Figure 12. Comparison between experimental and predicted values for the product size distribution of industrial surveys #6 (**a**), #3 (**b**), #5 (**c**) and #8 (**d**). Red dashed lines represent the distributions fitted separately for each industrial survey, while black lines represent the model predictions with the set of parameters in Table 5 and Equations (3)–(5).

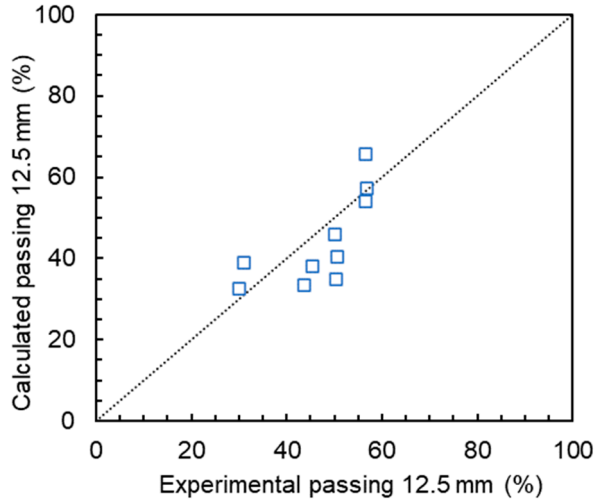


Figure 13. Comparison between experimental and calculated values for the percent passing 12.5 mm for all industrial surveys performed in the present work when using the set of parameters in Table 5 and Equations (3)–(5).

5. Conclusions

Ten industrial surveys performed over the period of several years of operation of the secondary crushing stages of the Minas Rio Plant (Anglo American), fed with a blend of Compact and Supercompact Itabirites, were used to assess the crusher performance under different feed characteristics and crushing conditions. Significant variations were observed in the performance of the crushers, with reduction ratios varying from 1.6 to 4.4. Nevertheless, a distinct non-normalizable breakage behavior was evident with an inflection point at around 240 μm. Details of the crusher power and throughput for the various industrial surveys also demonstrated important variabilities, associated with crushing conditions and feed size.

The application of the Andersen–Whiten crusher model, implemented in the commercial software Integrated Extraction Simulator (IES) from Orica Inc., first relied on the description of the normalized appearance (breakage) function based on drop-weight tests with particle sizes varying from 13.2–16.0 mm to 53–63 mm. The results showed a higher breakage intensity for the Compact Itabirite when compared to the Supercompact Itabirite, with $A \times b$ varying from 677.3 to 126.2, respectively. The t_{10}-t_n relationship was well grouped, and the incomplete beta function allowed the description of the data.

Classification function parameters were then fitted for each industrial survey separately by estimating parameters K_1 and K_2 on the basis of feed coarseness and closed-side setting. A modification to the model was implemented to account for the non-normalizable nature of the size reduction of the Itabirite iron ore, demonstrating the improved model prediction in the fine end of the product size distribution for the different industrial surveys. In order to obtain a single set of parameters that described the crushing response of the ore across all experimental campaigns, multiple linear regression was performed, and the optimal values of parameters that could describe the variation in K_1, K_2 and t_{10} as a function of operating conditions were fitted. A good agreement between the model and experiments for the different industrial survey campaigns was reached.

A model for predicting the maximum throughput of the crusher when operating in choke-feeding conditions was proposed from simulations in the software Bruno© (Version 4.2.2.0, exe v4.1.2.9, DB v9.50, Metso Corporation, Helsinki, Finland), from Metso, and information from crusher manuals. The model describes the throughput based on closed-side setting, ore bulk density, crushability, moisture content and feed coarseness. In spite of the empirical nature of the model, its robustness was demonstrated by predicting the HP500 cone crusher throughput with good confidence when compared to data from all industrial surveys.

Crusher power prediction demonstrated a limitation in the model by capturing variabilities in the different industrial surveys and of crushers operating in parallel that were surveyed, besides unaccounted fluctuations in the proportion of Compact and Supercompact Itabirites in the feed.

The application of this modified version of the Andersen–Whiten model is key for describing industrial-scale cone crushing of Itabirite iron ores by capturing the intrinsic non-normalizable breakage behavior of the material. The use of a throughput model is key for allowing a proper design and analysis of cone crushers operating in integrated circuits, besides allowing one to understand how to optimize crushing conditions to better capture the process dynamics of the crusher.

Author Contributions: Conceptualization, B.K.N.d.R., T.M.C. and L.M.T.; methodology, B.K.N.d.R., T.M.C. and J.S.; software, B.K.N.d.R. and T.M.C.; validation, B.K.N.d.R., T.M.C. and L.M.T.; formal analysis, B.K.N.d.R., T.M.C. and L.M.T.; investigation, B.K.N.d.R. and L.M.T.; data curation, B.K.N.d.R. and T.M.C.; writing—original draft preparation, B.K.N.d.R., T.M.C. and L.M.T.; writing—review and editing, B.K.N.d.R., T.M.C., L.M.T. and J.S.; visualization, B.K.N.d.R., T.M.C. and L.M.T.; supervision, L.M.T.; project administration, L.M.T.; funding acquisition, L.M.T. and J.S. All authors have read and agreed to the published version of the manuscript.

Funding: This research was funded by Anglo American (project PEMM23347), while additional funding was provided by the Conselho Nacional de Desenvolvimento Científico e Tecnológico (CNPq) through grant numbers 313425/2021-3 and 140276/2023-8.

Data Availability Statement: Data will be made available on request.

Acknowledgments: The authors are thankful for the technical and financial support from the Minas Rio personnel, besides permission from Anglo American to publish this work.

Conflicts of Interest: The authors declare no conflicts of interest.

Appendix A. Industrial Surveys

Table A1 presents the summary of the main operating conditions and feed characteristics of the industrial surveys that are part of the present work.

Table A1. Summary of operating conditions and feed characteristics for the different industrial surveys performed on HP500 cone crushers.

Industrial Survey #	80% Passing Size-f_{80} (mm)	Closed-Side Setting (mm)	Solid Feed Rate (t/h)	Power (kW) *
1	88	54	1639	209
2	84	54	1267	212
3	47	48	1240	262
4	88	48	1034	349
5	62	48	1124	325
6	79	40	813	355
7	140	38	1050	306
8	123	44	1138	325
9	81	40	820	350
10	81	55	1334	187

* Estimated based on electric current values.

Appendix B. Fitting of Throughput Model

As mentioned in Sections 2 and 4.3, the calibration of the throughput model (Equations (10)–(15)) was performed based on a reverse engineering approach with simulations performed in the software Bruno© [32] and information from crusher manuals [31]. The base case was assumed, as presented in Section 2.2, with granite with an impact work index of 16 kWh/t and solid and bulk densities of 2700 kg/m^3 and 1600 kg/m^3, respectively. The feed was considered to contain an 80% passing size of 100 mm and a moisture content of 1%, whereas the nominal closed-side setting was set to 38 mm in an HP500 cone crusher equipped with a medium cavity.

The results from Figure A1 show the relationship between the work index correction factor (β) when varying the work index from 7.3 to 30 kWh/t, which shows a clear power law relationship, through which the crusher throughput drops as the feed work index value increases. Differences between medium and fine cavities were not observed, whereas coarse and extra-coarse cavities, despite their similarity, presented slightly higher values for the work index correction factor (β) when compared to the former. The results from Bruno© and fitted values with Equation (12) presented a good agreement for simulations performed with the HP500 with medium and fine cavities, where the optimal value for parameter η is 0.15. Increments in crusher capacity when using coarse and extra-coarse cavities are not explicitly accounted for in Equation (12) and should be considered by selecting a suitable value of parameter λ in Equation (10).

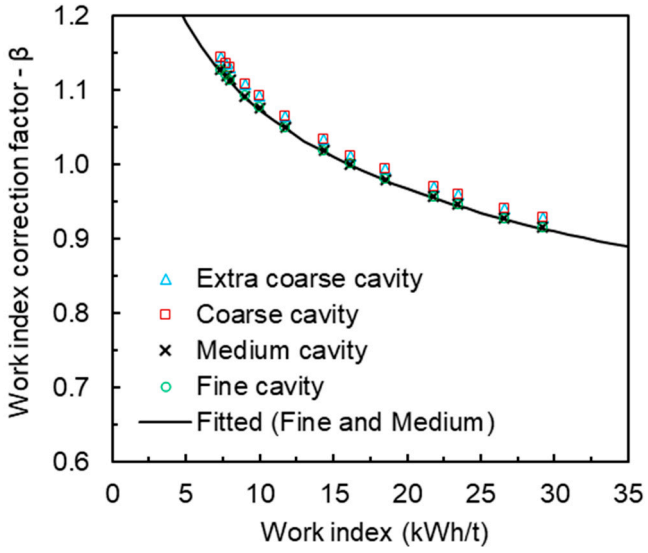


Figure A1. Variation in the work index correction factor (β) from Equation (12) as a function of the impact work index (Wi) for different crusher cavities.

The values of the feed coarseness correction factor (γ) as a function of 80% passing size in the feed (f_{80}) are presented in Figure A2 for different crusher cavities. As demonstrated in Figure A1, the results are divided into two groups with high similarity, namely medium and fine cavities and coarse and extra-coarse cavities. As expected, a clear reduction in crusher throughput is observed for coarser feed, with a drop of 20% in the feed coarseness correction factor (γ) when changing f_{80} from 60 to 180 mm in the HP500 crusher with a medium cavity. The results were well described by Equation (13) with an optimal value for parameter ε of 0.26 for medium and fine cavities and 0.15 for coarse and extra-coarse cavities. The results in Figure A2 are presented recognizing the maximum allowed feed sizes for the fine (f_{80} of 100 mm) and medium cavities (f_{80} of 140 mm) [31].

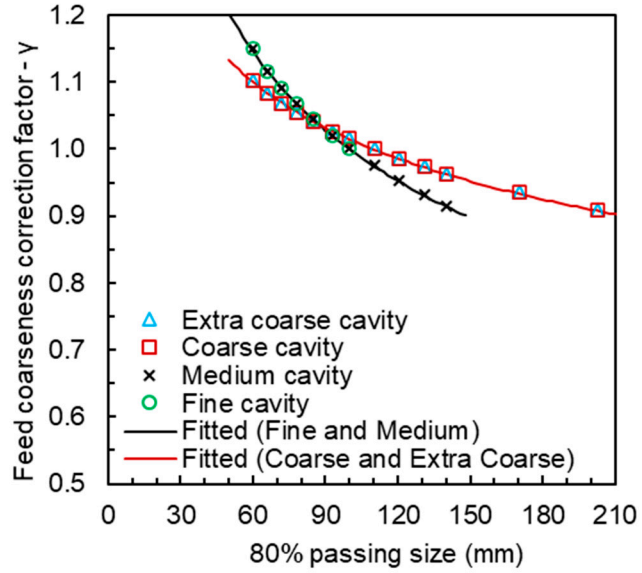


Figure A2. Variation in the feed coarseness correction factor (γ) from Equation (13) as a function of 80% passing size in the feed (f_{80}) for the HP500 crusher.

The variation in the feed moisture content correction factor (δ) from Equation (14) for moisture content from 1% to 5% is presented in Figure A3. The results were obtained from the crusher manual [31] and demonstrated a significant interaction with the closed-side

setting. The fitting of Equation (14) is presented in Figure A3, with good agreement with the model. It shows that throughput drops with the increase in feed moisture content, more so when the crusher operates at smaller CSS values.

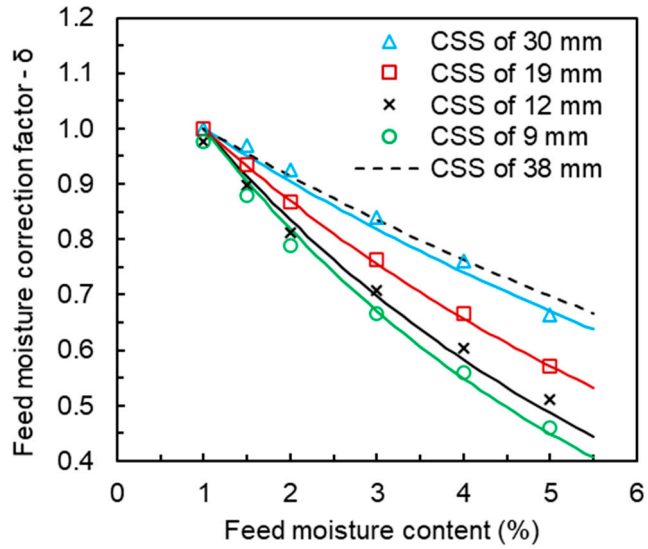


Figure A3. Variation in the feed moisture factor (δ) from Equation (14) as a function of the feed moisture content (ω) for different closed-side settings.

The optimal values of parameter ξ in Equation (14) varied according to CSS (Figure A3), and their relationship is presented in Figure A4, being represented by Equation (A1):

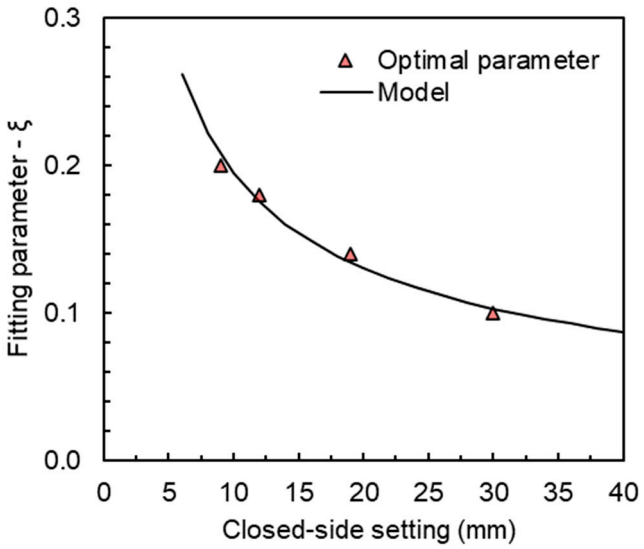


Figure A4. Variation in optimal values for parameter ξ from Equation (14) as a function of CSS. Solid line represents the fit to Equation (A1).

$$\xi_{Opt} = \left(\frac{\phi}{CSS}\right)^{\Omega} \tag{A1}$$

where ϕ and Ω are fitting parameters with optimal values of 0.595 and 0.580, respectively. From Equation (A1), it is then possible to estimate the optimal value of ξ to be used in Equation (14), which is given as 0.09. Thus, the correction factor accounting for the surface

moisture (δ) in Equation (14) may then be described as a function of both moisture content and closed-side setting as

$$\delta = \begin{cases} 1 & \text{for } \omega < 1\% \\ \exp\left[-\left(\frac{\phi}{CSS}\right)^{\Omega}(\omega - 1)\right] & \text{for } \omega \geq 1\% \end{cases} \quad \text{(A2)}$$

Finally, Figure A5 presents the relationship between the CSS correction factor (Ψ) and the CSS obtained from simulations in Bruno© for different crusher cavities, showing the significant increase in capacity with the increase in CSS. As observed in Figures A1 and A2, slight differences are observed when changing the crusher cavity from fine and medium to coarse and extra-coarse cavities. Figure A5 then presents the fit of Equation (15) to results from these two groups, with an optimal value of v of 1.27 for the fine/medium cavities and 1.19 for the coarse/extra-coarse cavities.

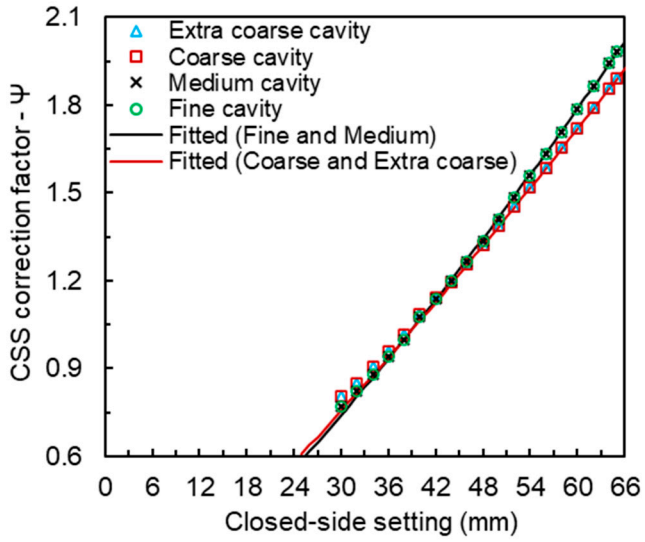


Figure A5. Variation in the optimal values for parameter CSS correction factor (Ψ) according to different values of CSS. The black line represents the fit corresponding to Equation (15) for fine and medium cavity, whereas the red line represents the fit corresponding to Equation (15) for coarse and extra-coarse cavities.

Appendix C. Fitting of Power Model

As mentioned in Section 2, Equation (8) requires as an input the energy matrix (Ecs_{t10_i}) for selected t_{10} values, and this input is summarized in Table A2. The data composing Table A2 were selected as an average of data obtained from DWTs with particle sizes of Compact and Supercompact Itabirites that are relevant for the crushing stage investigated in the present work.

Table A2. Summary of the energy matrix (Ecs_{t10_i}) for selected values of t_{10} used as input in Andersen–Whiten crusher model. Values are the specific energies in kWh/t.

t_{10} (%)	22.4 mm	31.5 mm	45.0 mm	63.0 mm
10	0.046	0.046	0.046	0.046
20	0.099	0.099	0.099	0.099
30	0.168	0.168	0.168	0.168

To estimate the crusher power, the present work used the predicted crusher capacity (Section 4.3) for each industrial survey campaign to calculate the power estimated based on drop-weight tests (Equation (8)). The no-load power was defined as one-third of the

installed power of the HP500 crusher, which is equal to 110 kW. The optimal value of parameter ζ in Equation (7) was given as 1.30 to properly describe the power consumption of different industrial surveys, which corresponds to a 77% efficiency. The results in Figure A6 show a comparison between experimental and calculated values for the crusher power for all industrial surveys, where a fair agreement between the model and experiments was achieved, indicating that while the correspondence is only fair, it is still found to be acceptable, given the lack of bias in the results. The results are presented with variations in the crusher power predicted by Bruno© with the coarsest (green line) and the finest (blue line) feed size distributions used in the present work (Table A1), which highlights that, despite the scatter, experimental and predicted values are within the typical range in operation. Crusher powers considered in Bruno© were obtained considering a solid feed rate of 1200 t/h, which was the average of the industrial surveys performed. For the specific cases of industrial surveys #1 and #2 (Table A1), it is worth noting that the measured values for the crusher power were below the expected values, and thus, they were disregarded in this analysis.

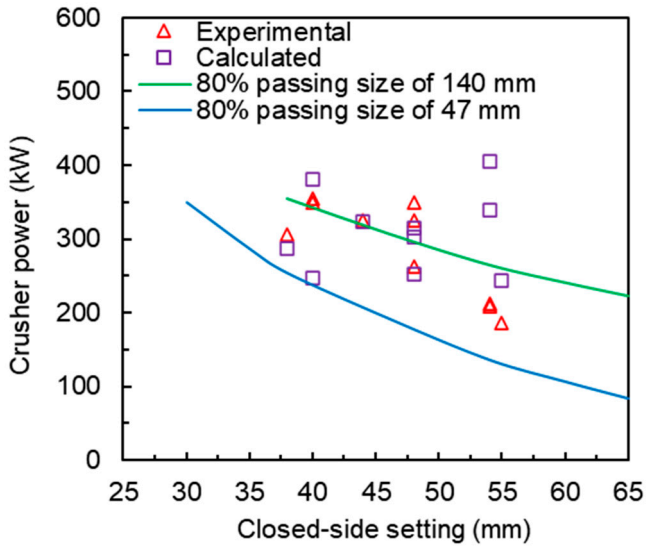


Figure A6. Comparison of calculated and experimental values for the crusher power in industrial surveys performed in the present work. Red triangles are experimental values and purple squares are calculated values, while green and blue lines are, respectively, the crusher powers obtained in Bruno© with the coarser and finer size distributions tested.

References

1. França, J.R.O.; Barrios, G.K.P.; Turrer, H.D.G.; Tavares, L.M. Comminution and liberation response of iron ore types in a low-grade deposit. *Miner. Eng.* **2020**, *158*, 106590. [CrossRef]
2. Carvalho, P.S.L.; Silva, M.M.; Rocio, M.A.R.; Moszkowicz, J. Biblioteca Digital—Minério de ferro. *Bndes Setorial* **2014**, *39*, 197–234.
3. Campos, T.M.; Bueno, G.; Barrios, G.K.P.; Tavares, L.M. Pressing iron ore concentrate in a pilot-scale HPGR. Part 2: Modeling and simulation. *Miner. Eng.* **2019**, *140*, 105876. [CrossRef]
4. Faria, P.M.C.; Rajamani, R.K.; Tavares, L.M. Optimization of solids concentration in iron ore ball milling through modeling and simulation. *Minerals* **2019**, *9*, 366. [CrossRef]
5. Rocha, B.K.N.; Campos, T.M.; Alves, L.P.; Silva, J.; Turrer, H.D.G.; Lichter, J.; Tavares, L.M. Multicomponent modeling and simulation of the Minas Rio iron ore grinding circuit. In Proceedings of the International Mining Processing Congress (IMPC) Asia-Pacific Conference 2022, Melbourne, Australia, 22–24 August 2022.
6. Rodrigues, A.F.D.V.; Delboni, H., Jr.; Powell, M.S.; Tavares, L.M. Comparing strategies for grinding itabirite iron ores in autogenous and semi-autogenous pilot-scale mills. *Miner. Eng.* **2021**, *163*, 106780. [CrossRef]
7. Whiten, W.J. The simulation of crushing plants with models developed using multiple spline regression. *J. South. Afr. Inst. Min. Metall.* **1972**, *72*, 257–264.
8. Yamashita, A.S.; Thivierge, A.; Euzébio, T.A. A review of modeling and control strategies for cone crushers in the mineral processing and quarrying industries. *Miner. Eng.* **2021**, *170*, 107036. [CrossRef]

9. Karra, V.K. A process performance model for cone crushers. In Proceedings of the 14th International Mineral Processing Congress, Toronto, ON, Canada, 17–23 October 1982; pp. 6.1–6.14.
10. King, R.P. Simulation - the modern cost-effective way to solve crusher circuit processing problems. *Int. J. Min. Process* **1990**, *29*, 249–265. [CrossRef]
11. Neves, P.B.; Tavares, L.M. Racionalização do uso da energia na britagem com auxílio de simulação computacional. *Tecnol. Em Metal. E Mater.* **2004**, *1*, 53–58. [CrossRef]
12. Andersen, J.; Napier-Munn, T.J. Power Prediction for Cone Crushers. In Proceedings of the Third Mill Operators Conference, Cobar, Australia, 9–12 May 1988; pp. 103–106.
13. Moshgbar, M.; Bearman, R.A.; Parkin, R. Optimum control of cone crushers utilizing an adaptive strategy for wear compensation. *Miner. Eng.* **1995**, *8*, 367–376. [CrossRef]
14. Magalhães, F.N.; Tavares, L.M. Rapid ore breakage parameter estimation from a laboratory crushing test. *Int. J. Miner. Process* **2014**, *126*, 49–54. [CrossRef]
15. Duarte, R.A.; Yamashita, A.S.; da Silva, M.T.; Cota, L.P.; Euzébio, T.A. Calibration and validation of a cone crusher model with industrial data. *Minerals* **2021**, *11*, 1256. [CrossRef]
16. Herbst, J.A.; Oblad, A.E. Modern control theory applied to crushing part 1: Development of a dynamic model for a cone crusher and optimal estimation of crusher operating variables. *IFAC Proc. Vol.* **1985**, *18*, 301–307. [CrossRef]
17. Machado Leite, M.R. Kinetic models for the simulation of crushing circuits. *Miner. Eng.* **1990**, *3*, 165–180. [CrossRef]
18. Evertsson, C.M. Cone Crusher Performance. Ph.D. Thesis, Chalmers University of Technology, Gothenburg, Sweden, 2000.
19. Cleary, P.W.; Sinnott, M.D.; Morrison, R.D.; Cummins, S.; Delaney, G.W. Analysis of cone crusher performance with changes in material properties and operating conditions using DEM. *Miner. Eng.* **2017**, *100*, 49–70. [CrossRef]
20. Cleary, P.W.; Morisson, R.D. Geometric analysis of cone crusher liner shape: Geometric measures, methods for their calculation and linkage to crusher behaviour. *Miner. Eng.* **2021**, *160*, 106701. [CrossRef]
21. André, F.P.; Tavares, L.M. Simulating a laboratory-scale cone crusher in DEM using polyhedral particles. *Powder Technol.* **2020**, *372*, 362–371. [CrossRef]
22. Jiang, C.; Gou, D.; Li, C.; Wu, G.; An, X.; Wang, J.; Guo, P. Crushing characteristics and performance evaluation of iron ore in a cone crusher: A numerical study. *Miner. Eng.* **2023**, *204*, 108429. [CrossRef]
23. Gauldie, K. The Output of gyratory crushers. *Engineering* **1954**, *4*, 557–559.
24. Evertsson, C.M. Output prediction of cone crushers. *Miner. Eng.* **1998**, *11*, 215–231. [CrossRef]
25. Napier-Munn, T.J.; Morrell, S.; Morrison, R.D.; Kojovic, T. *Mineral Comminution Circuits: Their Operation and Optimisation*, 1st ed.; Julius Kruttschnitt Mineral Research Centre: Queensland, Australia, 1996.
26. Narayanan, S.S.; Whiten, W.J. Determination of comminution characteristics from single particle breakage tests and its application to ball mill scale-up. *Trans. Instn. Min. Met.* **1988**, *97*, 115–124.
27. King, R.P. *Modeling and Simulation of Mineral Processing Systems*, 1st ed.; Elsevier: Amsterdam, The Netherlands, 2001.
28. Campos, T.M.; Bueno, G.; Tavares, L.M. Modeling comminution of iron ore concentrates in industrial-scale HPGR. *Powder Technol.* **2021**, *383*, 244–255. [CrossRef]
29. Bilgili, E.; Toprak, A.; Altun, D.; Altun, O. PBM of an industrial-scale vertical wet stirred media mill (HIGMill): Assessment of back-calculation and hybrid methods. *Powder Technol.* **2024**, *440*, 119760. [CrossRef]
30. Tavares, L.M. Review and further validation of a practical single-particle breakage model. *KONA Powder Part. J.* **2022**, *39*, 62–83. [CrossRef]
31. Metso. *Crushing Manual*, 6th ed.; Metso Minerals: Helsinki, Finland, 2005.
32. Metso. *Bruno: Process Simulation Software for Optimizing Aggregate Production*; Version 4.2.2.0, exe v4.1.2.9, DB v9.50; Metso Corporation: Helsinki, Finland, 2021.
33. Bergstrom, B.H. Crushability and grindability. In *SME Mineral Processing Handbook*; Weiss, N.L., Ed.; Society for Mining Metallurgy: Englewood, CO, USA, 1985; pp. 30–68.
34. Tavares, L.M.; Carvalho, R.M. Impact work index prediction from continuum damage model of particle fracture. *Miner. Eng.* **2007**, *20*, 1368–1375. [CrossRef]
35. Carvalho, R.M.; Secchi, A.; Tavares, L.M. A new energy-based breakage function model and optimization procedure for mechanistic comminution models. In Proceedings of the 14th European Symposium on Comminution and Classification, Gothenburg, Sweden, 7–11 September 2015; pp. 1–4.
36. Tavares, L.M. Breakage of Single Particles: Quasi-Static. In *Handbook of Powder Technology*; Elsevier: Amsterdam, The Netherlands, 2007; Volume 12, pp. 3–68.
37. Tavares, L.M. Role of particle microstructure in comminution. *Dev. Miner. Process.* **2000**, *13*, C4–C99.
38. Tavares, L.M.; Neves, P.B. Microstructure of quarry rocks and relationships to particle breakage and crushing. *Int. J. Miner. Process* **2008**, *87*, 28–41. [CrossRef]
39. Chikochi, C. Ore breakage characterisation of UG2 deposits using the JK RBT. Master's Thesis, University of Cape Town, Cape Town, South Africa, 2017.

40. Austin, L.G.; Luckie, P.T. The estimation of non-normalized breakage distribution parameters from batch grinding tests. *Powder Technol.* **1972**, *5*, 267–271. [CrossRef]
41. Wills, B.A.; Napier-Munn, T. *Wills' Mineral Processing Technology: An Introduction to the Practical Aspects of Ore Treatment and Mineral Recovery*, 7th ed.; Elsevier: Amsterdam, The Netherlands, 2006.

Disclaimer/Publisher's Note: The statements, opinions and data contained in all publications are solely those of the individual author(s) and contributor(s) and not of MDPI and/or the editor(s). MDPI and/or the editor(s) disclaim responsibility for any injury to people or property resulting from any ideas, methods, instructions or products referred to in the content.